Acta Mechanica 163, 25–38 (2003)
DOI 10.1007/s00707-003-1018-1

Acta Mechanica
Printed in Austria

Elastomer bushing response: experiments and finite element modeling

J. Kadlowec, Glassboro, New Jersey, and **A. Wineman** and **G. Hulbert**, Ann Arbor, Michigan

Received January 13, 2003
Published online: May 20, 2003

Summary. Elastomer bushings are essential components in tuning suspension systems since they isolate vibration, reduce noise transmission, accommodate oscillatory motions and accept misalignment of axes. This work presents an experimental study in which bushings are subjected to radial, torsional and coupled radial-torsional modes of deformation. The experimental results show that the relationship between the forces and moments and their corresponding displacements and rotations is nonlinear and viscoelastic due to the nature of the elastomeric material. An interesting feature of the coupling response is that radial force decreases and then increases with torsion. The experimental results were used to assess bushing behavior and to determine the strength of radial-torsional coupling. The experimental results were also compared to finite element simulations of a model bushing. While finite element analysis predicted small displacements at the relaxed state reasonably well, the response to larger radial deformations and coupled deformations was not well captured.

1 Introduction

A bushing is typically composed of a hollow elastomer cylinder contained between inner and outer cylindrical steel sleeves. These sleeves connect components of the suspension system; forces are transmitted across the connection through the elastomeric material, which reduces shock and vibration. During normal use, the bushing sleeves undergo displacements and rotations relative to one another about axes both along and perpendicular to the centerline of the sleeves. The most prevalent modes of deformation in an automotive suspension, which are the basis for this study, include radial, torsional and combined radial-torsional deformations. The radial mode is defined as a translation of one sleeve relative to the other sleeve in which each point moves an equal distance perpendicular to the centerline. The torsional mode is defined as a rotation of one sleeve relative to the other sleeve about the centerline.

The elastomeric bushings of interest in this study are used in automotive suspension systems and are of mold bonded type. Due to the nature of the elastomeric material, the relation between the forces and moments and their corresponding displacements and rotations is nonlinear and time dependent. Further nonlinearities have also been found to exist due to coupling between different modes of deformation.

Finite element analysis is a commonplace tool in component design, yet this computational tool has limitations for bushing design. One limitation is the amount of available material data for the wide variety of materials used in automotive components. The compounds have different response due to changes in fillers, processing and curing. Determining accurate

material model parameters requires significant testing of material samples and materials characterization. Currently material parameters are determined from tension, compression, equibiaxial tension and pure shear tests which are relatively simple tests to conduct. The choice of tests and ranges of deformation affect the resulting material parameters, which is why it is important to test elastomer samples under the types and ranges of deformations that the elastomer component will be subjected to in application. Deformation histories of bushings and other elastomer components often are quite complex, so material parameters determined from relatively simple test deformations have difficulties in capturing the response due to complex deformations.

Some published works related to bushing research are available in the literature. An empirical model for the design of shear bushings by Petek [1], uniaxial elastic load-deflection relations by Adkins [2] and Hill [3]–[5] and finite element analyses for bushing design (Morman [6]) are the apparent extent of earlier works in modeling bushing response. These works do not include both time effects of the elastomeric material and coupled modes of deformations.

Determining a load-deformation relation for bushings from constitutive, compatibility and equilibrium equations for bushing material produces a nonlinear boundary value problem, which involves large, time consuming calculations, relative to the overall size and time required to perform multibody dynamics simulations of vehicles. For this reason, Wineman proposed a direct relation between force and displacement in bushings, which incorporates nonlinear and viscoelastic effects [8]. The model has the form of a nonlinear, single integral expression for the force in terms of the displacement histories. It depends on a displacement dependent force relaxation function, a bushing property determined from experimental data. Lee showed that bushing response obtained using this proposed force-displacement relation agrees well with the response determined by solving the boundary value problem for axial, torsional, and coupled modes, at least for short time events [9]. This work was then extended for modeling the radial, torsional and coupled radial-torsional deformation modes [10].

The purpose of this paper is to present an experimental program for testing elastomer bushings, to present experimental results for bushing response due to single and coupled deformation modes, and to compare the elastic bushing response with finite element results for bushing behavior. The paper begins with brief descriptions of the test specimens, experimental facilities and preconditioning of samples. The test programs for both the single and coupled mode deformation experiments are described, specifically the experimental program that was conducted in order to determine the nature of force response for radial, torsional and combined radial-torsional displacement control tests. Representative experimental force-deformation and force-time results, which illustrate nonlinear and viscoelastic properties, are presented and discussed. Finite element modeling and analysis of a bushing using different forms for the material model are presented. The experimental results for the relaxed state of the bushing were compared with finite element simulations for the model bushing. The similarities and differences between experimental and finite element modeling results are discussed.

2 Experiments

The ideal process to calculate bushing force response is to determine a material constitutive law and solve an appropriate boundary value problem. This continuum mechanics approach is not always practical and still requires experiments to validate the model. For these reasons, bypassing the continuum mechanics approach and determining a force-deformation relation

directly is desirable. A relatively specialized yet thorough experimental program is employed to provide the necessary data to determine a force-deformation relation [10]. Bushing force and/or moment response is measured for radial, torsional and coupled radial-torsional deformations.

2.1 Test samples and equipment

The test samples were provided by Tenneco Automotive - Clevite Elastomers. The samples are a variation of a production mold bonded bushing used in automotive suspension systems. Mold bonded bushings are manufactured by injection molding the elastomeric material between inner and outer metal sleeves. The elastomeric material cures and adheres to the metal sleeves during vulcanization. The bushing is then swaged, i.e. the outer metallic sleeve is radially compressed. The radial compression is performed to eliminate the tensile stresses induced by the shrinking of the elastomer during curing and improve durability. The inner and outer sleeves are made of steel, and the elastomer is a carbon-black filled natural rubber, which is 60 durometer after curing. The initial outer radius of the elastomer is 19.05 mm. The final dimensions of the elastomer after swaging are 60 mm length, 18.2 mm outer radius and 9.85 mm inner radius (Fig. 1).

A computer controlled Instron 8511 multi-axis servo-hydraulic test machine was used to perform quasi-static and dynamic displacement control tests on the samples. The servo-hydraulic actuators that are mounted on two perpendicular axes are capable of providing linear translational and rotational motions along each axis (Fig. 2). Each linear actuator has a plus/minus 50.8 mm stroke and a 24.5 kN force capacity. Each rotary actuator has a plus/minus 50 degree angle of rotation and a 565 N-m torque capacity. The four actuators are controlled by Instron Model 8511 console towers, one for each of the actuators. Each actuator can be operated independently or operated simultaneously with the others using either displacement or load control. An IBM compatible 486/33 MHz computer is connected to the Instron Model 8511 consoles through an IEEE-488 GPIB bus. This connection allows the computer to control displacements during tests and acquire data via the Instron control software FLAPS5. Data acquisition rates were limited to 200 Hz due to the computer speed and available RAM. Load and torque measurements were taken with Sensotec transducers and corresponding amplifiers. Fixturing was designed for the machine to accommodate independent, as well as combined, radial and torsional deformations of the bushing. A critical issue was to minimize misalignments in the two axes, which would create uncertainties in the experimental results.

2.2 Preconditioning of samples

The elastomer material in bushings consists of natural rubber and large amounts of carbon black filler. Breakdown of the weak bonds occurs between rubber molecules and filler particles and

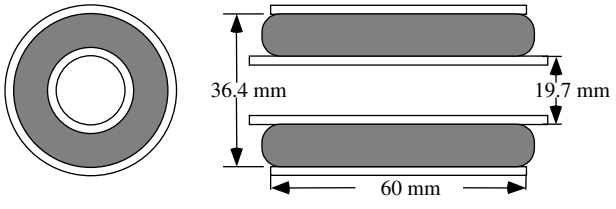

Fig. 1. Schematic of bushing sample

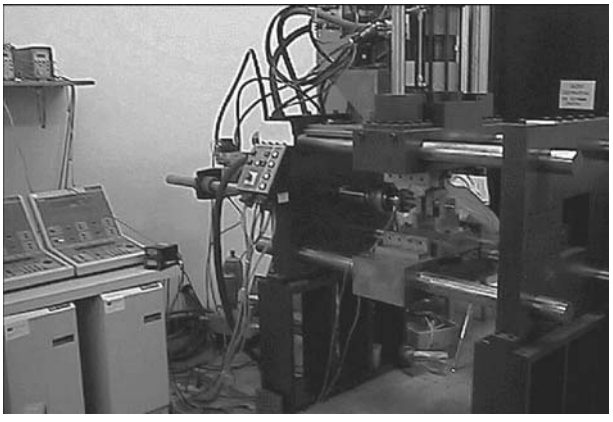

Fig. 2. Bushing test machine

between the rubber molecules at crosslinks. The degree of breakdown in the elastomer is most significant during the first exercise of the bushing, which then stabilizes. This causes the bushing response in subsequent loadings to be softer than that of the first cycle. This phenomenon of change in material behavior due to prior deformation is known as the Mullins effect [11], [12]. In practice a bushing is not loaded only once, so taking data during the first loading cycle would not capture typical bushing response. In order to avoid the unsteady structure of the material immediately after production or after prolonged periods of rest, the test piece was subjected to several cycles of loading before actual testing. This procedure is referred to as preconditioning.

The amount of preconditioning followed a typical procedure used by Tenneco Automotive for static rate testing. A prescribed displacement was applied at a rate of 0.0833 mm/second for the radial tests or an angle was applied at a rate of 1 degree/second for the torsional tests. Preconditioning consisted of three cycles at an amplitude of 115 percent of the test displacement amplitude to be prescribed. After this preconditioning, material effects were considered to be the same for each test.

While factors such as aging, amplitude and frequency of loading, and temperature do affect conditioning and degradation of the elastomeric material over time, they were not considered in this study. Since the previously mentioned breakdown appears to occur quite slowly provided that no extreme loading conditions are imposed on the bushing, it was assumed that the microstructure of the elastomeric bushing remained fairly constant during testing. Limitations of the test machine did not allow for temperature control, so studies of temperature effects were not possible. However, the room temperature was 23 ± 2 degrees Celsius over the course of testing, and the tests results were repeatable within this temperature range.

To avoid variability in results due the set-up, each sample was kept in the test fixturing for the duration of a given suite of tests. Each sample was allowed to recover for 45 minutes between tests during each day of testing. If a sample had not been tested or at least cycled within a 24 hour period, then the bushing was conditioned again before running another test.

3 Experimental results

3.1 One-dimensional tests and results

One-dimensional tests, consisting of radial or torsional (Fig. 3) deformation modes and histories, were performed on a set of axisymmetric, mold-bonded bushings. The radial displace-

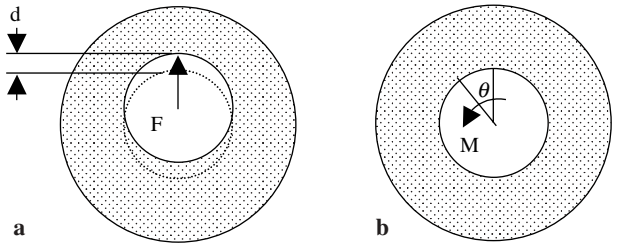

Fig. 3a. Radial, and **b** torsional modes of deformation

ment control tests were conducted by supporting the inner sleeve by the shaft and displacing the outer sleeve relative to the inner sleeve. The load transducer mounted to the vertical axis measured the radial force response. The torsional tests were conducted by holding the outer sleeve fixed and rotating the inner sleeve. A torque transducer mounted in line on the horizontal axis measured moment response.

An ideal type of bushing test is the step displacement or rotation. Force relaxation response to a step displacement is the ideal method for determining parameters in the bushing model of Wineman [6] and determining the initial and relaxed response. However, due to inertia of the testing equipment, a true step displacement test is not physically possible, so a ramp to constant displacement test was used instead. The test controller was programmed to increase displacement at a constant rate during a period from time zero to a rise time of T*. Once T* was reached, the displacement was held constant for 20 seconds. By decreasing T*, the ramp to constant value test (Fig. 4) approaches a step displacement test. Tests were conducted for a variety of rise times ranging from 0.1 to 8.0 seconds and radial displacements of 0.2 to 1.2 mm or torsional rotations of 5 to 25 degrees.

Figure 5 shows the force-time histories of the bushing sample under radial deformation. A radial displacement was imposed at a constant rate until a final displacement of 1.0 mm was achieved. For each test in the series, the deformation rate was increased (i.e., the rise time decreased), and thus, the final displacement was reached in a shorter time. The rise times employed were 0.1, 0.2, 0.5, 1, 2, 4, and 8 seconds.

Several important phenomena are observed from the force response data. For each of the ramp to constant displacement tests, the peak force occurs at T* and this peak is greatest for the shortest rise time. The force relaxes to an equilibrium during the period in which the displacement remains constant. The difference between the peak loads at the shortest and longest rise times is approximately ten percent of the relaxed load. This rate dependence is an expected characteristic for viscoelastic materials. Long molecular chains of rubber require time to slip past one another. Entanglements can occur between and along molecular chains, thus the material behaves as though the chains are shorter. If the sample is deformed at a rate faster than the chains can slip past one another, the material behaves as though the chains are shorter (i.e., the material has a stiffer response). Due to fading memory of the material, it can be seen that after a short period of time all of the force responses relax to the same equilibrium value.

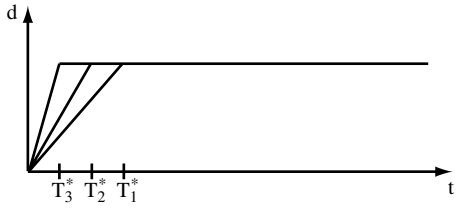

Fig. 4. Ramp to constant displacement history

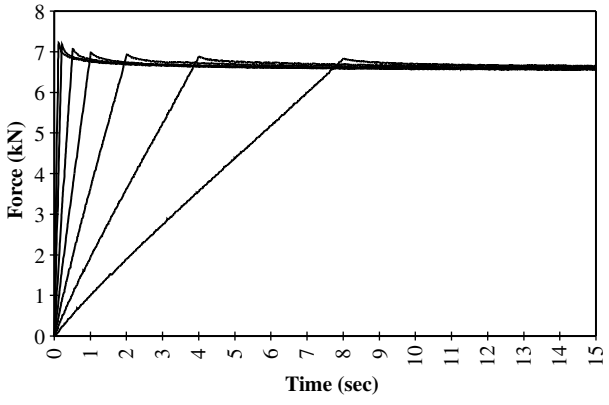

Fig. 5. Representative radial force relaxation responses for ramp to constant displacement tests, d = 1.0 mm

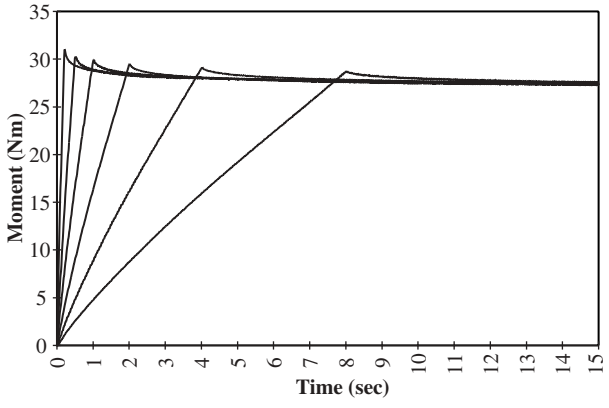

Fig. 6. Representative relaxation moment response for ramp to constant angle tests, ϕ = 15 deg

The peak loads, relaxed loads and characteristic relaxation times are the important features needed for modeling the bushing response.

Figure 6 shows the moment responses from ramp to constant rotation of 15 degrees at rise times of 0.2, 0.5, 1, 2, 4, and 8 seconds. The torsional moment response has features similar to those for the radial force response. Both the radial and torsional test responses almost reached the fully relaxed state within 20 seconds. After 20 seconds, the force or moment response was within 2 percent of the fully relaxed value. In automotive applications, loading events occur on short time scales, thus the bushing response beyond this time were ignored.

Nonlinearity is revealed in isochrones of radial and torsional responses. The radial step tests were conducted for final displacements between 0.2 and 1.2 mm, and the relaxed radial force at t = 20 seconds is plotted as a function of the corresponding displacement in Fig. 11, experimental data. The torsional step tests were conducted for rotations between 5 and 25 degrees, and the relaxed moment at t = 20 seconds is plotted as a function of the corresponding angular rotation in Fig. 12, experimental data. Both curves are s-shaped, indicating that the force-displacement and moment-rotation responses are nonlinear, which is the typical behavior for rubberlike materials. The decrease in shear stiffness at small deformations is due to the filler-rubber interactions. Stiffness then increases at larger deformations due to finite extensibility of the network chains [13], [14]. The force-displacement curve shows only a slight amount of nonlinearity, while the moment-angle curve shows considerably more softening behavior.

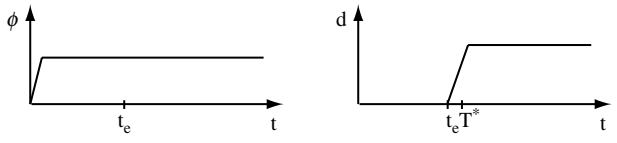

Fig. 7. Deformation history for the two successive steps – rotation, θ, followed by radial displacement, d

3.2 Coupled tests and results

The coupled tests consisted of combinations of the one-dimensional tests. Again, a series of ramp to constant displacement tests at decreasing rise times was conducted. The ramp to constant rotation was imposed on one axis and the moment was allowed to relax to an equilibrium. The second axis was then subjected to the ramp to constant deformation. Figure 7 shows a typical deformation history for the two successive steps. The constant deformation values tested were combinations of the one-dimensional values and were imposed with a rise time of 0.2 seconds. The coupled responses were compared to the results of the one-dimensional responses in order to show the strength of coupling, assess the role of time effects and determine bushing properties for coupled mode deformations.

One important observation from the radial-torsional test results is that the radial force response is affected by a torsional preset. Figure 8 shows radial force versus angle of rotation data. Each data point represents the relaxed radial force due to a radial displacement of 0.2 mm and each of the various angles of rotation. As the angle increases, the radial force response to a prescribed displacement first decreases, then increases. Initially, the radial force decreases as the preset angle is increased from zero to 10 degrees. The radial force then increases as the preset angle is further increased from 10 to 20 degrees.

Figure 9 shows the radial force versus angle of rotation for a variety of radial displacements at a relaxed time of t = 20 seconds. Each data point represents the difference between the radial force at a given radial displacement and angle of zero degrees and the radial force at the same given radial displacement and some nonzero angle. The data is represented this way so that the absolute force difference due to an angle change could be assessed, and the curves for all values of displacement scaled on the same plot. This plot shows that as the angle increases, the radial force response to a prescribed displacement first decreases then increases, with the minimum occurring at 10 to 15 degrees regardless of the level of radial displacement.

Work by Yeoh [15] provides some insight into the material behavior that produces this bushing behavior. Network crosslinks and entanglements are speculated to induce softening at

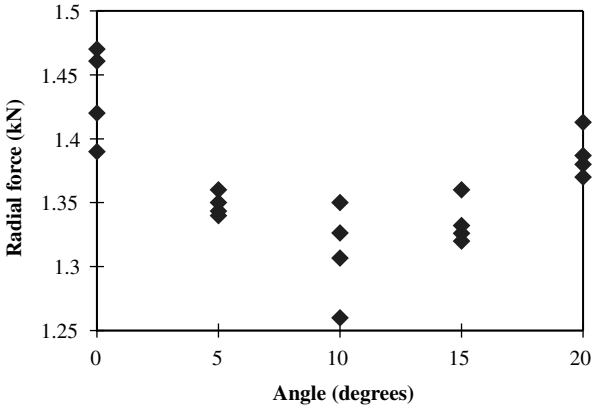

Fig. 8. Radial force due to 0.2 mm displacement at t = 20 seconds versus preset angle

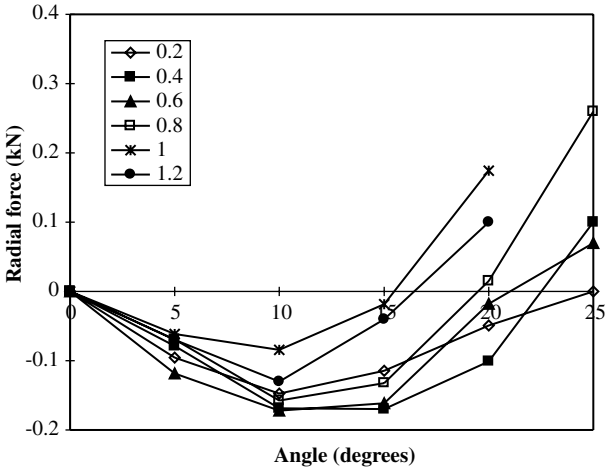

Fig. 9. Difference in radial force for various displacements versus preset angle at t = 20 seconds

small strains. Relating this to the case at hand, as the preset is increased, the shear strain due to the rotational deformation causes a softening behavior (i.e., decrease of radial force). Yeoh presumes that finite extensibility of network chains causes stiffening behavior at large strains. So, as the preset angle is further increased, the finite extensibility explains the stiffening behavior (i.e., increase of radial force). Manufacturing processes may also contribute to some of these effects, since the swaging operation induces a compressive prestress in the radial direction and adds to the complexity of the deformations.

4 Comparison with finite element simulations

The finite element method is a popular tool for designing elastomeric components. This numerical method approximates the stress/strain behavior of rubber components based on a theoretical material model. The bushing under investigation was modeled using finite elements. Global response was analyzed and compared to experimental force-deformation response. Assumptions about the local stress/strain behavior were made from the analysis.

4.1 Bushing finite element model

The bushing was modeled as a hollow cylinder consisting of solid "hybrid" elements, C3D8H elements in ABAQUS, 8 radially, 36 circumferentially and 15 axially. A fixed boundary condition was prescribed on the outer surface nodes of the model. Each of the inner surface nodes at the inner sleeve radius was connected to a slave node with a beam multi-point constraint; this allowed for a force or displacement condition to be prescribed on the inner surface via this slave node. Since the bushing is symmetric about the plane perpendicular to the bushing axis for the loading cases studied, only half of the length of the bushing was modeled. ABAQUS Standard was the solver used to compute the resultant forces, stresses and displacements for the various loading conditions.

While there are many constitutive laws for nonlinear finite-deformation elastic analysis, the bushing response was computed using three forms of a strain energy potential, which are available in ABAQUS: Standard – Ogden, polynomial and Arruda-Boyce forms [16]. Let λ_i,

where $i = 1, 2, 3$ be the principal stretch ratios and $J = \lambda_1\lambda_2\lambda_3$, then the deviatoric principal stretch ratios are defined as $\bar{\lambda}_i = J^{-1/3}\lambda_i$. The Ogden strain energy potential is

$$U = \sum_{i=1}^{N} \frac{2\mu_i}{\alpha_i^2}\left(\bar{\lambda}_1^{\varepsilon_i} + \bar{\lambda}_2^{\varepsilon_i} + \bar{\lambda}_3^{\varepsilon_i} - 3\right), \tag{1}$$

where μ_i and α_i are temperature dependent material parameters. The parameters for a third order Ogden model are listed in Table 1.

The polynomial strain energy potential is

$$U = \sum_{i+j=1}^{N} C_{ij}\left(\bar{I}_1 - 3\right)^i\left(\bar{I}_2 - 3\right)^j, \tag{2}$$

where C_{ij} are material parameters, and $\bar{I}_1$ and $\bar{I}_2$ are the first and second strain invariants

$$\bar{I}_1 = \bar{\lambda}_1^2 + \bar{\lambda}_2^2 + \bar{\lambda}_3^2, \tag{3}$$

$$\bar{I}_2 = \bar{\lambda}_1^2\bar{\lambda}_2^2 + \bar{\lambda}_2^2\bar{\lambda}_3^2 + \bar{\lambda}_3^2\bar{\lambda}_1^2. \tag{4}$$

The third invariant is $\bar{I}_3 = \bar{\lambda}_1\bar{\lambda}_2\bar{\lambda}_3 = 1$, which is the incompressibility constraint. Table 2 lists the parameters for the polynomial form.

The Arruda-Boyce strain energy potential is

$$\begin{aligned} U = \mu\Bigg\{&\frac{1}{2}\left(\bar{I}_1 - 3\right) + \frac{1}{20\lambda_m^2}\left(\bar{I}_1^2 - 9\right) + \frac{11}{1050\lambda_m^4}\left(\bar{I}_1^3 - 27\right) \\ &+ \frac{19}{7050\lambda_m^6}\left(\bar{I}_1^4 - 81\right) + \frac{519}{673750\lambda_m^8}\left(\bar{I}_1^5 - 243\right) + \ldots\Bigg\}, \end{aligned} \tag{5}$$

where μ and λ_m are material parameters, and $\bar{I}_1$ is the first invariant

Table 1. Material parameters for Ogden form

i	μ_i	α_i
1	1.061898	0.428246
2	0.0578289	5.71269
3	0.0159176	−4.59726

Table 2. Material parameters for polynomial form

C_{10}	0.545816
C_{01}	−0.020755
C_{20}	0.003668
C_{11}	0.0048571
C_{02}	0.
C_{30}	−0.0001415
C_{21}	0.
C_{12}	0.

$$\bar{I}_1 = \bar{\lambda}_1^2 + \bar{\lambda}_2^2 + \bar{\lambda}_3^2. \tag{6}$$

The material parameters have the values $\mu = 0.85354$ and $\lambda_m = 2.2053$.

The material parameters for each of the forms of strain energy potentials are representative of the elastomer from which the bushings are manufactured. For the three material models considered here, the stress-strain response due to the typical homogeneous deformations are plotted in Fig. 10. Note that all of the material models predict similar behavior for these simple modes of deformation, particularly at small strains. For uniaxial tension, the Ogden and Arruda-Boyce models predict similar behavior of S-shaped stress-strain curves, while the polynomial model does not exhibit this. Under biaxial extension, the Arruda-Boyce and polynomial forms are nearly identical, but the Ogden form predicts a significantly stiffer response than both of these. The planar shear response is nearly identical for all material models. While these differences are relatively small for these simple test cases and the small strains (less than 50 percent strain) that the bushings undergo, the finite element analysis shows that the differences due to coupled modes of deformation are more significant.

The finite element simulation for radial and torsional deformations on the bushing was conducted after first simulating the prestress due to the cool and swage procedure. The initially prestressed model has a half length of 29.4 mm, an inner radius, R_i, of 9.85 mm, and an outer radius, R_o, of 19.05 mm, which are the dimensions of the molded bushing. The cooling and swaging procedures were simulated. The initial temperature was set at 160 degrees Celsius to simulate the mold temperature. The first step in the computation was to simulate cooling by reducing the temperature of the nodes to 20 degrees Celsius. This resulted in residual tensile forces throughout the bushing model. Holding the inner surface fixed, the next step in the analysis consisted of displacing the outer radius nodes radially inward by 0.85 mm in order to

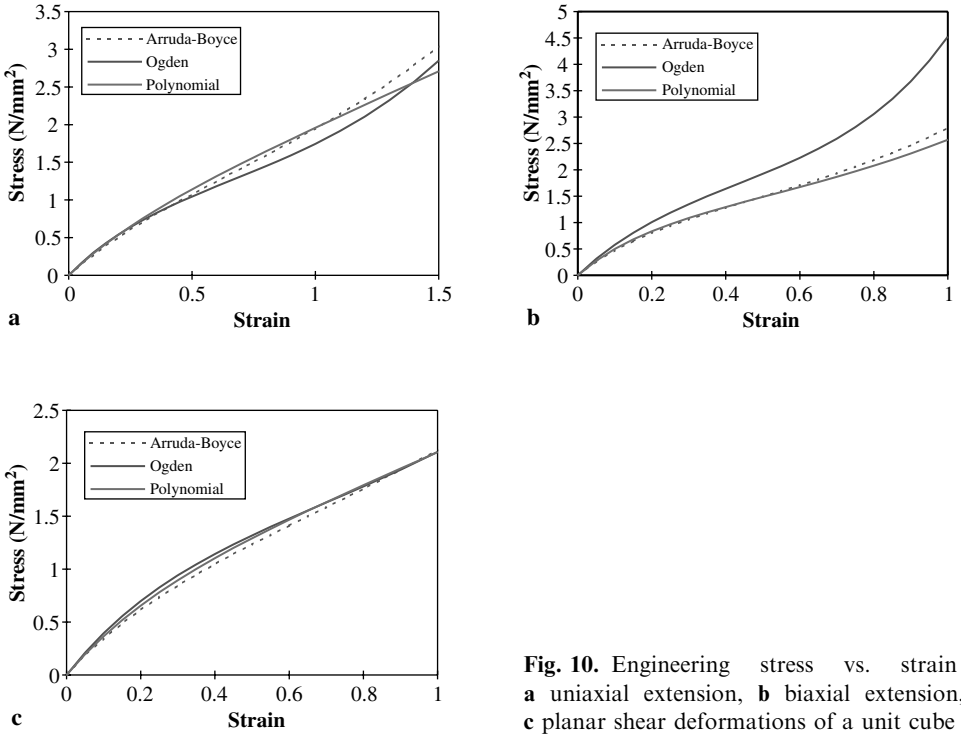

Fig. 10. Engineering stress vs. strain for **a** uniaxial extension, **b** biaxial extension, and **c** planar shear deformations of a unit cube

simulate the swaging procedure to the final part dimensions. This resulted in a compressive stress in the bushing model that is greatest along the symmetry plane and becomes less compressive along the length of the bushing, where the elastomer bulges out of the free ends of the bushing.

The prestressed models for bushings using each of the material models were first analyzed to assess the effects on each of the single mode deformations. Figure 11 shows the radial force-deformation curves for the bushing models for the different material strain energy functions along with the relaxed experimental data. An initial observation is that the radial force and torsional moment are significantly greater in the bushing model with the Ogden material model. For each form of the material models, the force in the radial direction at large displacements is overestimated. Quantitatively, the polynomial form better predicts the experimental force. An important difference to note is that the experimental curve is nonlinear, while the computational curves are approximately linear. The slope of the experimental curve for the radial deformation first softens then stiffens, but the slopes of the computational curves are slightly increasing.

Figure 12 shows the torsional moment-rotation curves for bushing models using the different material strain energy functions along with the experimental data. Here the experimental curve lies between the curves which were generated from computational data. Again the experimental curve shows distinct nonlinearity. The Ogden material model predicts a slight softening as displacement increases, while the polynomial material model predicts a fairly linear response. Quantitatively, the Ogden model produces a better fit for small angles of rotation, while the polynomial and Arruda-Boyce models produce a better fit at larger angles.

The bushing finite element models were next analyzed using each of the materials to assess the coupling effects for combined radial and torsional deformations. Figure 13 shows the radial force versus angle of rotation for the finite element models using the different material strain energy functions and the corresponding experimental results. Each data point represents the radial force due to a radial displacement of 0.4 mm and each of the various angles of rotation. The coupled behavior is quite different for each of the material models. Using the Ogden form for strain energy, the force decreases at first as the angle of rotation increases and then stiffens as the angle is further increased. Qualitatively, these computational results capture the type of behavior that is seen experimentally, but quantitatively the effect is much

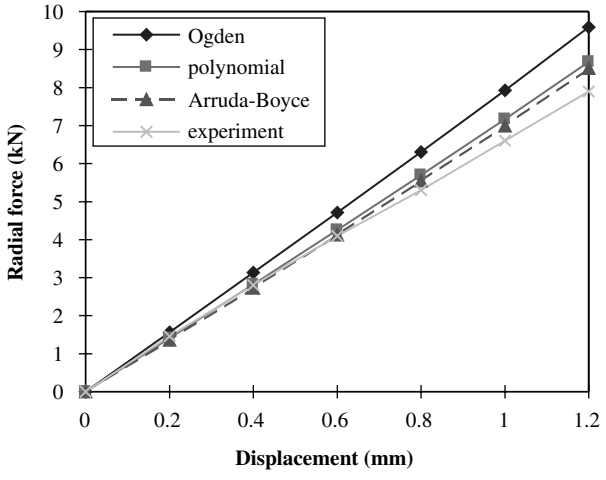

Fig. 11. Computed and experimental radial forces versus radial displacements

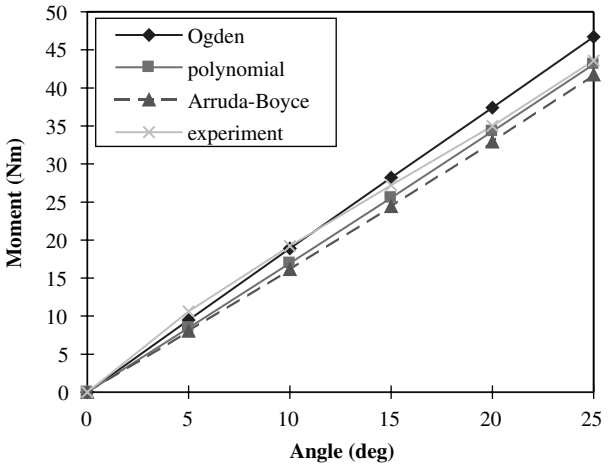

Fig. 12. Computed and experimental torsional moments versus angular rotations

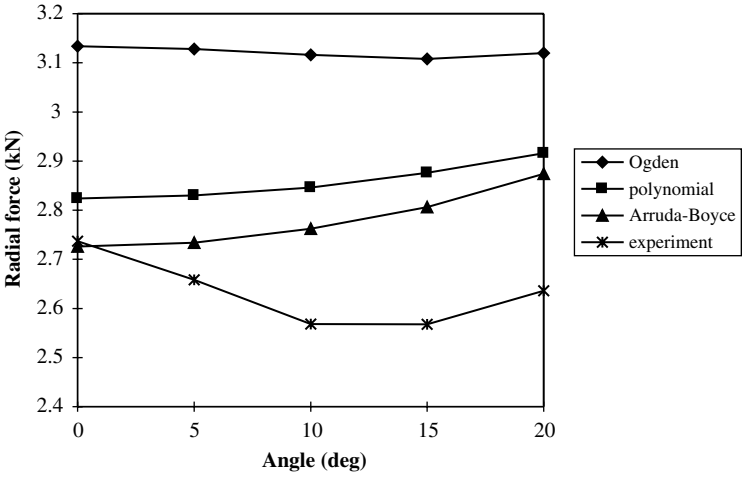

Fig. 13. Computed and experimental radial forces versus angle for radial displacement = 0.4 mm

larger experimentally, and the actual value of radial force is less for the experiments. Using the polynomial and Arruda-Boyce forms, the radial force always increases as the angle of rotation increases for all levels of radial displacement and rotation angles in this study. The increase in radial force due to a change in angle is greater for the Arruda-Boyce material than for the polynomial material. This is evident by noting that the Arruda-Boyce parameters are positive, thus strain energy, and subsequently force and stress, increase with increasing deformation. Ogden and polynomial have negative parameters, which allow for some decrease in the strain energy for increasing deformations. The behavior predicted by Arruda-Boyce and polynomial models is not seen experimentally, but the actual values of radial force for experiments and computation with these models are reasonably close, which was also the case for the single mode deformations.

The Ogden material model appears to best capture the bushing response in the finite element study. While discrepancies exist between experimental data and computational results using the Ogden material model, the Ogden model qualitatively captures the trend for the coupled radial-torsional response that the other material models do not. Recall that Fig. 9 shows the

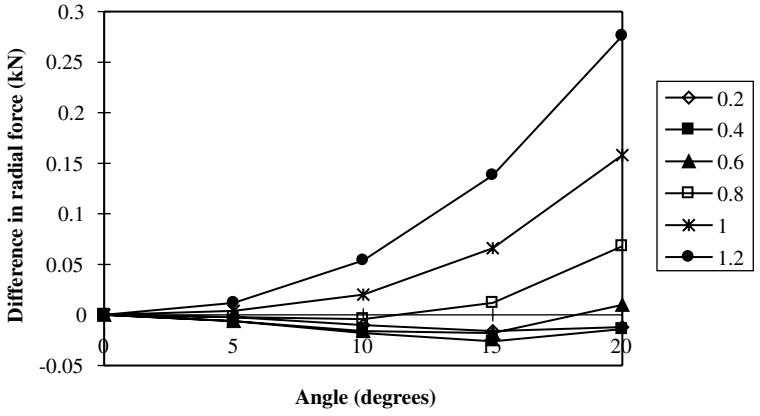

Fig. 14. Difference in computed radial forces at various displacements versus angles

experimentally measured difference in radial force versus angle of rotation for a variety of radial displacements. Figure 14 shows the computed difference in radial force versus angle of rotation for a variety of radial displacements. In both Figs. 9 and 14, the quantity on the vertical axis is the difference in radial force at a given radial displacement and an angle of zero degrees subtracted from the radial force at the same given radial displacement and some nonzero angle. This was done so that the absolute force difference due to an angle change could be assessed and so that radial force curves for all values of displacement could be scaled on the same plot. The trend for coupled radial-torsional behavior does appear in the finite element results but is not as pronounced as the experimental results indicate. The experimental results show that a significant softening occurs for preset angles less than or equal to 10 degrees. The finite element results show a slight softening in radial force due to preset angle, but only stiffening at larger radial deformations. The amount of stiffening at the larger radial displacements and angles of rotation is then overestimated by the finite element model. Due to the disparity between the relaxed results for the experiments and finite element analysis, modeling of the viscoelastic response was not pursued as a part of this study.

5 Conclusions

In order to determine the mechanical behavior of the bushing, a thorough experimental investigation was conducted on elastomeric bushings, which was presented. The experimental program consisted of radial and coupled radial-torsional displacement control tests. The experimental results show the nonlinear, viscoelastic bushing behavior under single mode and coupled mode deformations. An interesting feature of the coupling response is that radial force at a given radial displacement first decreases as the angle of preset increases and then increases with further angle increase.

A finite element analysis was conducted to determine the elastic bushing response due to radial, torsional and coupled modes of deformation. While computational results are in reasonable agreement for the single deformation modes, there are qualitative differences in the response due to coupled modes of deformation. The bushing finite element model using the Ogden material model qualitatively captured the softening-stiffening effect of preset torsion on radial response, while the other material models did not. While finite element analysis is a useful tool in the design of bushings and other components, further studies are necessary to make this

an accurate tool. An important consideration is the testing used for the material characterization. The testing procedure should consist of a wide variety of deformations that account for the deformations that a particular bushing is subjected to in applications. Conducting tension, compression and shear tests and combinations of these are important in order to accurately determine the mechanical response. Further, processing of elastomer materials impacts the mechanical behavior of the material, so test samples for material characterization should be molded in the same fashion as the actual bushing.

Acknowledgements

The authors would like to thank Tenneco Automotive and the Great Lakes Truck and Transit Research Center for support of this project.

References

[1] Petek, N.K., Kicher, T.P.: An empirical model for the design of rubber shear bushings. Rubber Chemistry and Technology **60**, 298–309 (1987).
[2] Adkins, J.E., Gent, A.N.: Load-deflexion relations of rubber bush mountings. British J. Appl. Phys. **5**, 354–358 (1954).
[3] Hill, J.M.: Radial deflections of thin precompressed cylindrical rubber bush mountings. Int. J. Solids Struct. **13**, 93–104 (1977).
[4] Hill, J.M.: Radial deflections of rubber bush mountings of finite length. Int. J. Engng Sci. **13**, 407–422 (1975).
[5] Hill, J.M.: The effect of precompression on the load-deflection of long rubber bush mountings. J. Appl. Polymer Sci. **19**, 747–755 (1975).
[6] Morman, K.N., Pan, T.Y.: Application of finite-element analysis in the design of automotive components. Rubber Chemistry and Technology **61**, 503–533 (1988).
[7] Chen, C.K., Wu., C.T.: On computational issues in large deformation analysis of rubber bushings. Mech. Struct. Mach. **33**, 327–349 (1997).
[8] Wineman, A.S., VanDyke, T., Shi, S.: A nonlinear viscoelastic model for one-dimensional response of elastomeric bushings. Int. J. Mech. Sci. **40**, 1295–1305 (1998).
[9] Lee, S.B.: A study of a nonlinear viscoelastic model of elastomeric bushing response. PhD Diss., The University of Michigan, 1997.
[10] Kadlowec, J.A.: Radial and torsional coupling in elastomeric bushings. PhD Diss., The University of Michigan, 1999.
[11] Mullins, L.: Effect of stretching on the properties of rubber. J. Rubber Res. **16**, 275–289 (1947).
[12] Mullins, L.: Hysteresis in tension tests. Trans. Inst. Rubber Industry **23**, 280–287 (1948).
[13] Mullins, L.: Determination of degree of crosslinking in natural rubber vulcanizates, Part IV. Stress-strain behavior at large extensions. J. Appl. Polymer Sci. **2**, 257–263 (1959).
[14] Mullins, L.: Softening of rubber by deformation. Rubber Chemistry Technology **42**, 339–362 (1969).
[15] Yeoh, O.H.: Some forms of the strain energy function for rubber. Rubber Chemistry Technology **66**, 754–771 (1993).
[16] ABAQUS User's Manual, Pawtucket, MA, Hibbitt, Karlsson & Sorensen (1999).

Authors' addresses: J. Kadlowec, Rowan University, Glassboro, NJ 08028 (E-mail: kadlowec@rowan.edu); A. Wineman and G. Hulbert, University of Michigan, Ann Arbor, MI 48109-2125, U.S.A.